mathematics

MDPI

Article

The Hybrid Modeling of Spatial Autoregressive Exogenous Using Casetti's Model Approach for the Prediction of Rainfall

Annisa Nur Falah [1,*], Budi Nurani Ruchjana [2], Atje Setiawan Abdullah [3] and Juli Rejito [3]

[1] Doctoral Program of Mathematics, Faculty of Mathematics and Natural Sciences, Universitas Padjadjaran, Sumedang 45363, Indonesia
[2] Department of Mathematics, Faculty of Mathematics and Natural Sciences, Universitas Padjadjaran, Sumedang 45363, Indonesia; budi.nurani@unpad.ac.id
[3] Department of Computer Science, Faculty of Mathematics and Natural Sciences, Universitas Padjadjaran, Sumedang 45363, Indonesia; atje.setiawan@unpad.ac.id (A.S.A.); juli.rejito@unpad.ac.id (J.R.)
* Correspondence: annisa15046@mail.unpad.ac.id

Abstract: Spatial Autoregressive (SAR) models are used to model the relationship between variables within a specific region or location, considering the influence of neighboring variables, and have received considerable attention in recent years. However, when the impact of exogenous variables becomes notably pronounced, an alternative approach is warranted. Spatial Expansion, coupled with the Casetti model approach, serves as an extension of the SAR model, accommodating the influence of these exogenous variables. This modeling technique finds application in the realm of rainfall prediction, where exogenous factors, such as air temperature, humidity, solar irradiation, wind speed, and surface pressure, play pivotal roles. Consequently, this research aimed to combine the SAR and Spatial Expansion models through the Casetti model approach, leading to the creation of the Spatial Autoregressive Exogenous (SAR-X) model. The SAR-X was employed to forecast the rainfall patterns in the West Java region, utilizing data obtained from the National Aeronautics and Space Administration Prediction of Worldwide Energy Resources (NASA POWER) dataset. The practical execution of this research capitalized on the computational capabilities of the RStudio software version 2022.12.0. Within the framework of this investigation, a comprehensive and integrated RStudio script, seamlessly incorporated into the RShiny web application, was developed so that it is easy to use.

Keywords: SAR-X; Casetti's model; climate variables; prediction; RShiny

MSC: 9004; 62M30

Citation: Falah, A.N.; Ruchjana, B.N.; Abdullah, A.S.; Rejito, J. The Hybrid Modeling of Spatial Autoregressive Exogenous Using Casetti's Model Approach for the Prediction of Rainfall. *Mathematics* **2023**, *11*, 3783. https://doi.org/10.3390/math11173783

Academic Editors: Qun Li and Aihua Wood

Received: 22 July 2023
Revised: 30 August 2023
Accepted: 1 September 2023
Published: 3 September 2023

1. Introduction

Water is very important for all living organisms, including humans, thereby ranking as one of the most indispensable resources in the environment [1]. The phenomenon of climate change and global warming has significantly reshaped numerous environmental aspects across multiple countries. This transformation carries the potential for profound consequences, imperiling the populace, agriculture, ecosystems, economy, and industry. Alterations in precipitation patterns exert a direct impact on the management of water resources, agricultural practices, hydrological systems, and ecological balance [2]. It is crucial to acknowledge that the entirety of life-sustaining water on Earth originates from rainfall. Consequently, comprehending the spatial distribution and fluctuations in this rainfall is very important. This understanding is pivotal for efficient water resource management and also for devising strategies for addressing challenges such as anticipating natural hazards triggered by intense rainfall events [1,3,4]. Delving into the spatial arrangement and variances of rainfall can play a pivotal role in shaping perspective notions concerning water resources. Furthermore, it aids in formulating measures for upholding

stable environmental circumstances. It is imperative to acknowledge that trends in rainfall constitute a pivotal climate determinant with far-reaching implications, encompassing future factors such as population growth, economic expansion, and enduring climatic shifts. These factors collectively impact both the temporal and spatial availability of water [1,5,6].

In various spheres of life, the anticipation of rainfall yields indispensable advantages, encompassing agriculture, water resource management, disaster preparedness, infrastructure planning, renewable energy, and transportation. Forecasts of rainfall assist farmers in coordinating their planting and harvesting schedules, allowing for effective irrigation planning, suitable crop selection according to weather conditions, and a decreased risk of crop failure [7–9]. Moreover, these predictions contribute to the proficient handling of water resources, encompassing the regulation of river flow and reservoir management [10,11]. The availability of accurate rainfall information empowers optimal water utilization and mitigates flood and drought hazards, as well as plays a pivotal role in the management of natural calamities such as floods and landslides [12–14]. Informed by projected rainfall data, authorities can implement preventive measures such as early evacuation, timely alerts, and the construction of robust infrastructure. Additionally, rainfall prediction has proved vital in the realm of infrastructure planning, guiding the construction of structures including dams, drainage networks, and irrigation channels [15–17]. By leveraging rainfall insights, engineers and planners are equipped to devise designs resilient to extreme weather conditions. Rainfall profoundly affects renewable energy industries, namely hydropower and solar energy [18]. Forecasts of rainfall facilitate the strategic planning and management of renewable energy production, thereby optimizing energy potential [19]. The influence of rainfall extends to transportation planning as well [20]. Intense rainfall impacts road traffic, transportation speeds, and driver safety. By leveraging rainfall predictions, transportation schedules can be organized more efficiently, ultimately reducing accident risks. The availability of accurate rainfall information empowers sound decision making and aids in mitigating the risks and repercussions arising from unforeseen weather fluctuations [21]. Therefore, the precision and accuracy of rainfall prediction are said to be important.

Based on previous research, diverse rainfall predictions have been undertaken, including projections of rainfall variability, particularly focusing on the winter and pre-monsoon rainfall across Pakistan [22]. In Turkey, monthly and seasonal rainfall trend predictions were calculated through a comparison of three interpolation methods, namely Inverse Distance Weighted, Completely Regularized Spline, and Ordinary Kriging [23]. A Spatial Autoregressive model was employed to predict seasonal legume yields for non-irrigated croplands in the semi-arid region of Mexico, categorized by regular rainy and dry seasons [24]. The rainfall and groundwater patterns along the northeastern coast of Brazil were predicted, and the monthly rainfall patterns were characterized to mitigate their impacts during heavy rainfall periods and significant floods, utilizing the Kriging method and a clustering analysis [25]. Additionally, short-term rainfall forecasts were derived using a Hierarchical Bayesian model for spatiotemporal data [26]. It is important to note that the scope of these predictions exclusively pertains to rainfall variability and does not encompass other climate variables.

One of the outcomes of climate phenomena is La Niña, which triggers heightened rainfall in the western Pacific region. Based on empirical data from BMKG, La Niña can amplify the rainfall in West Java by anywhere from 20% to 70% [27]. Rainfall is intertwined with other climatic factors such as air temperature, humidity, solar irradiation, wind speed, and surface pressure, all of which fluctuate across different areas [28]. The climate variables pertinent to specific regions or locations can be effectively modeled using a spatial analysis approach. Among the spatial models commonly employed, the Spatial Autoregressive (SAR) model stands out. This is frequently referred to as a mixed regressive spatial autoregressive model or a spatial lag model [29]. The SAR model, a statistical tool, is harnessed to depict the relationships between variables within a given region or location, considering the impacts of surrounding variables. However, the model falls short in capturing the spatial disparities between locations. To address this gap,

Casetti [30] developed the Spatial Expansion model, which extends the SAR to encompass exogenous variables through a linear regression approach. The amalgamation of the SAR and spatial expansion models, in line with the approach of Casetti, culminates in the Spatial Autoregressive Exogenous (SAR-X) model. The SAR-X introduces spatial heterogeneity, thereby enabling the description of distinct parameter values for each spatial observation, determined by the geographical distances between locations. A notable application of the SAR-X is evident in gauging the repercussions of climate change on the ecosystem of a region. For example, when analyzing flood risk prediction within the SAR-X framework, it becomes imperative to incorporate climate variable factors. In this scenario, the model serves as a valuable tool, facilitating an elevated spatial perspective of climate effects and accounting for the spatial influences that shape relationships. In essence, SAR-X modeling has emerged as a valuable instrument for comprehending the ramifications of climate change and supporting decision making to tackle these consequences.

The current research on rainfall prediction entails observations across 13 climate-monitoring stations in the West Java region, utilizing data sourced from the Meteorology, Climatology, and Geophysics Agency (BMKG) with location indexing. The research variables comprised rainfall as the responsive parameter, coupled with exogenous variables encompassing air temperature, humidity, solar irradiation, wind speed, and surface pressure. These climate data were procured from the National Aeronautics and Space Administration Prediction of Worldwide Energy Resources (NASA POWER) dataset. The application study in this research is supported by computing using the R programming language. R is a statistical and graphical programming language; currently, R is widely known as one of the programming languages used for data analysis and data science. R has advantages, including being open source, having many packages available, finding it easy to transform and process data, and being able to create interactive applications/web-based dashboards. In this research, the RStudio software is used, which is an Integrated Development Environment (IDE) for R [31]. The custom-built RStudio script can be further evolved into a web application employing RShiny version 1.7.4, one of the packages of software specifically designed for creating interactive web interfaces [32]. These web applications, once deployed, offer a user-friendly platform for data processing. Users can conveniently upload data for analysis, and the ensuing results are promptly presented on the RShiny web application interface. In this research endeavor, integrated commands within R script enable the utilization of the SAR-X model through the RShiny web application, rendering the process effortlessly accessible.

2. Materials and Methods

2.1. Inverse Distance Weight Matrix

The spatial weight matrix is a matrix that states the proximity relationship between locations. In this study, the inverse distance weight matrix, also called the distance weight, is used, which describes the actual distance between locations. The distance between locations is calculated using the latitude and longitude coordinates of the center point of the observed location. It is known that a location $x_{ij}(u_{ij}, v_{ij})$ with x_{ij} is the symbol of the location i and j, with $i = 1, 2, 3 \ldots, N$ and $j = 1, 2, 3 \ldots, N$, while u and v indicate the latitude and longitude coordinates. If d_{ij} is the distance between location i and location j, and W_{ij} is the inverse value of d_{ij}, we use the Euclidean distance and the equation is as follows [33]:

$$d_{ij} = \sqrt{\left(x_i(u_i) - x_j(u_j)\right)^2 + \left(x_i(v_i) - x_j(v_j)\right)^2} \quad (1)$$

$$w_{ij} = \begin{cases} \frac{1}{d_{ij}}, i \neq j \\ 0, i = j \end{cases} \quad (2)$$

Next, if the sum of the distance weights of a row in the inverse distance weight matrix is not equal to 1, then the distance weights must be standardized, so as to obtain $\sum_{j=1}^{N} w_{ij} = 1, \forall\, i = 1,2,3,\ldots,N$, where:

$$w_{ij}^{*} = \frac{w_{ij}}{\sum_{j=1}^{N} w_{ij}}, \forall\, i = 1,2,3,\ldots,N. \tag{3}$$

In detail:
x_{ij}: the symbol of location i and j, with $i = 1,2,3\ldots,N$ and $j = 1,2,3\ldots,N$
u_i: latitude $i-$ th for $i = 1,2,3,\ldots,N$
v_i: longitude $i-$ th for $i = 1,2,3,\ldots,N$
u_j: latitude $j-$ th for $j = 1,2,3,\ldots,N$
v_j: longitude $j-$ th for $j = 1,2,3,\ldots,N$
d_{ij}: the distance between location i and location j
In this investigation, the inverse distance weight matrix was employed to calculate the climate variable data across 13 climate observation stations in the West Java region. The input coordinates for each location, expressed as latitude and longitude, served to establish the proximity relationship between these locations.

2.2. Moran Index

One approach to assessing the spatial dependencies among locations is through a spatial autocorrelation test using the Moran Index statistic. Spatial autocorrelation gauges the correlation between observation values concerning the location of the same variable. When a systematic pattern emerges in the distribution of a variable, spatial autocorrelation is present. This phenomenon underscores the interdependence of the spatial data between different locations, influenced by their proximity or intersection [29].

$$I = \frac{n\sum_{i=1}^{n}\sum_{j=1}^{n} w_{ij}(x_i - \overline{x})(x_j - \overline{x})}{\sum_{i=1}^{n}\sum_{j=1}^{n} w_{ij}\sum_{i=1}^{n}(x_i - \overline{x})^2} \tag{4}$$

The hypothesis formulation in this test is as follows:
$H_0 : I = 0$ There is no spatial autocorrelation between locations.
$H_1 : I \neq 0$ There is spatial autocorrelation between locations.
The test statistic employed is expressed below:

$$Z(I) = \frac{I - E(I)}{\sqrt{Var(I)}} \approx N(0,1) \tag{5}$$

with,

$$E(I) = -\frac{1}{n-1} \tag{6}$$

$$Var(I) = \frac{n^2 S_1 - nS_2 + 3S_0^2}{(n^2-1)S_0^2} - [E(I)]^2 \tag{7}$$

$$S_0 = \sum_{i=1}^{n}\sum_{j=1}^{n} w_{ij} \quad S_1 = \frac{1}{2}\sum_{1\neq j}^{n}(w_{ij} + w_{ji})^2 \quad S_2 = \sum_{i\neq j}^{n}\left(\sum_{i=1}^{n} w_{ij} + \sum_{j=1}^{n} w_{ji}\right)^2$$

where:
I: the Moran Index value
n: the number of observation locations

x_i: the value of the observation variable at location $i-$ th
x_j: the value of the observation variable at location $j-$ th
$\overline{x}$: the average of the number of variables
w_{ij}: the elements of the standardized weight matrix between regions i and j
Decision:
Reject H_0 at the significance level α if $-Z_{score} \leq -Z_{\frac{\alpha}{2}}$ or $-Z_{score} \geq Z_{\frac{\alpha}{2}}$.

The Moran Index was in the range of $[-1, 1]$. A negative value signified a negative spatial autocorrelation, while a positive value implied a positive spatial autocorrelation [34].

2.3. Spatial Autoregressive Exogenous (SAR-X)

Spatial regression is a method tailored for data with spatial effects, encompassing spatial dependency and heterogeneity. Spatial dependence pertains to observations at one location being influenced by those at another, while spatial heterogeneity arises due to random location effects. The foundation of spatial regression lies in the classical linear regression method, evolving to consider the influence of space on the data under scrutiny. The first Law of Geography by Tobler emphasizes interconnectedness and the greater influence of nearby entities [29]. The general model of spatial regression can be written as follows:

$$\begin{gathered} \mathbf{y} = \rho \mathbf{W}\mathbf{y} + \mathbf{X}\boldsymbol{\beta} + \mathbf{u} \\ \mathbf{u} = \lambda \mathbf{W}\mathbf{u} + \boldsymbol{\varepsilon} \text{ with } \boldsymbol{\varepsilon} \overset{iid}{\sim} N\left(0, \boldsymbol{\sigma}^2 \mathbf{I}\right) \end{gathered} \tag{8}$$

In [29], an alternative model derived from Equation (8) was developed. When $\rho \neq 0$ and $\lambda = 0$, then the Spatial Autoregressive (SAR) model can be formed as follows:

$$\mathbf{y} = \rho \mathbf{W}\mathbf{y} + \mathbf{X}\boldsymbol{\beta} + \boldsymbol{\varepsilon} \text{ with } \boldsymbol{\varepsilon} \overset{iid}{\sim} N(0, \sigma^2 \mathbf{I}) \tag{9}$$

The SAR model, an area-based spatial model, encompasses the impact of spatial lag on the dependent variable [29].

The introduction of the Spatial Expansion model (Casetti, 1972) [30] addresses spatial heterogeneity, which characterizes diverse parameter values for each spatial observation based on the distance between locations. The Euclidean distance, such as location coordinates, quantifies the separation between two locations. The Spatial Expansion model, adopting a linear regression approach, can be formulated as follows:

$$\begin{gathered} \mathbf{y} = \mathbf{X}\boldsymbol{\beta} + \boldsymbol{\varepsilon} \text{ with } \boldsymbol{\varepsilon} \overset{iid}{\sim} N(0, \sigma^2 \mathbf{I}) \\ \boldsymbol{\beta} = \mathbf{Z}\mathbf{J}\boldsymbol{\beta}_\mathbf{0} \end{gathered} \tag{10}$$

In this research, a fusion of the SAR and Spatial Expansion models was executed, utilizing the approach of Casetti on exogenous variables, called the Spatial Autoregressive Exogenous (SAR-X) model. The SAR-X model could be said to be an extension of SAR, which encompasses exogenous variables. Referring to [35], the SAR-X model served to describe and predict independent variables, considering location effects and exogenous variables. Mathematically, the SAR-X model prediction with the Casetti's model approach was derived by substituting Equation (10) into (9), in order to produce the following:

$$\mathbf{y} = \rho \mathbf{W}\mathbf{y} + \mathbf{X}\boldsymbol{\beta} + \boldsymbol{\varepsilon} \text{ with } \boldsymbol{\beta} = \mathbf{Z}\mathbf{J}\boldsymbol{\beta}_0 \tag{11}$$

Equation (11) is subsequently written as:

$$\mathbf{y} = \rho \mathbf{W}\mathbf{y} + \mathbf{X}\mathbf{Z}\mathbf{J}\boldsymbol{\beta}_0 + \boldsymbol{\varepsilon} \text{ with } \boldsymbol{\varepsilon} \overset{iid}{\sim} N(0, \sigma^2 \mathbf{I}) \tag{12}$$

with:
$\mathbf{y}$: the vector of the dependent variables of size $(n \times 1)$
ρ: the spatial lag parameter coefficient of the independent variable
$\mathbf{W}$: a spatial weight matrix of size $(n \times n)$

X: the matrix of the independent variables of size $(n \times nk)$

Z: location information that contains elements Z_{xi}, Z_{yi} with $i = 1, \ldots, n$, representing the latitude and longitude of each observation, of size $(nk \times 2nk)$

J: the expansion of the identity matrix of size $(2nk \times 2k)$

$\boldsymbol{\beta}$: a matrix of size $(nk \times 1)$, containing parameter estimators for all the explanatory k variables at each observation

$\boldsymbol{\beta_0}$: parameter expressed by $\boldsymbol{\beta}_{latitude}, \boldsymbol{\beta}_{longitude}$ of size $(2k \times 1)$

$\otimes$: the Kronecker product

$\boldsymbol{\varepsilon}$: an error vector of size $(n \times 1)$

$\mathbf{s_i}$: the location matrix with $i = 1, \ldots, n$

The matrix form in the model can be written as follows:

$$\mathbf{y} = \begin{pmatrix} y(s_1) \\ y(s_2) \\ \vdots \\ y(s_n) \end{pmatrix}, \mathbf{W} = \begin{pmatrix} 0 & w_{12} & \ldots & w_{1n} \\ w_{21} & 0 & \ldots & w_{2n} \\ \vdots & \vdots & \ddots & \vdots \\ w_{n1} & w_{n2} & \ldots & 0 \end{pmatrix}, \mathbf{X} = \begin{pmatrix} x_{11} & \cdots & x_{1k} & 0 & \cdots & 0 & \cdots & 0 & \cdots & 0 \\ 0 & \cdots & 0 & x_{21} & \cdots & x_{2k} & 0 & \vdots & \cdots & \vdots \\ \vdots & \ddots & \vdots & 0 & \ddots & 0 & \ddots & 0 & \ddots & 0 \\ 0 & \cdots & 0 & 0 & \cdots & 0 & 0 & x_{n1} & \cdots & x_{nk} \end{pmatrix}$$

$$\boldsymbol{\beta} = \begin{pmatrix} \beta_1(s_1) \\ \beta_1(s_2) \\ \vdots \\ \beta_k(s_n) \end{pmatrix}, \boldsymbol{\varepsilon} = \begin{pmatrix} \varepsilon(s_1) \\ \varepsilon(s_2) \\ \vdots \\ \varepsilon(s_n) \end{pmatrix}, \boldsymbol{\beta_0} = \begin{pmatrix} \boldsymbol{\beta}_{latitude} \\ \boldsymbol{\beta}_{longitude} \end{pmatrix}$$

$$\mathbf{Z} = \begin{pmatrix} Z_{x1} \otimes \mathbf{I}_k & Z_{y1} \otimes \mathbf{I}_k & 0 & 0 & 0 & 0 \\ 0 & 0 & \ddots & \ddots & 0 & 0 \\ 0 & 0 & 0 & 0 & Z_{xn} \otimes \mathbf{I}_k & Z_{yn} \otimes \mathbf{I}_k \end{pmatrix}, \mathbf{J} = \begin{pmatrix} \mathbf{I}_k & 0 \\ 0 & \mathbf{I}_k \\ \vdots & \vdots \\ 0 & \mathbf{I}_k \end{pmatrix}$$

2.4. Estimation

The random error variable in the SAR-X model assumed a normal distribution. Therefore, the parameter estimation in this model followed the SAR parameter estimation method, employing the Maximum Likelihood Estimation (MLE) technique. The observed sources for this approach included Ord [36], Smirnov and Anselin [37], Robinson and Rossi [38], and Feng [39]. Equation (12) can be written as the following equation:

$$\mathbf{y} = \rho\mathbf{W}\mathbf{y} + \mathbf{A}\boldsymbol{\beta}_0 + \boldsymbol{\varepsilon} \text{ with } \mathbf{A} = \mathbf{XZJ} \tag{13}$$

$$\mathbf{y} = \rho\mathbf{W}\mathbf{y} + \mathbf{A}\boldsymbol{\beta}_0 + \boldsymbol{\varepsilon} \text{ with } \boldsymbol{\varepsilon} \overset{iid}{\sim} N(0, \sigma^2\mathbf{I}) \tag{14}$$

The probability density function used is expressed below:

$$f(\mathbf{y}) = \left(\frac{1}{2\pi\sigma^2}\right)^{\frac{n}{2}} \exp\left[-\frac{(\mathbf{y} - \rho\mathbf{W}\mathbf{y} - \mathbf{A}\boldsymbol{\beta}_0)^T(\mathbf{y} - \rho\mathbf{W}\mathbf{y} - \mathbf{A}\boldsymbol{\beta}_0)}{2\sigma^2}\right] \tag{15}$$

The likelihood function of the dependent variable $\mathbf{y}$ is formulated as follows:

$$\begin{aligned} L(\rho, \boldsymbol{\beta}_0|\mathbf{y}) &= f(\mathbf{y}|\rho, \boldsymbol{\beta}_0) \\ &= \left(\tfrac{1}{2\pi\sigma^2}\right)^{\frac{n}{2}} \exp\left[-\tfrac{(\mathbf{y} - \rho\mathbf{W}\mathbf{y} - \mathbf{A}\boldsymbol{\beta}_0)^T(\mathbf{y} - \rho\mathbf{W}\mathbf{y} - \mathbf{A}\boldsymbol{\beta}_0)}{2\sigma^2}\right] \end{aligned} \tag{16}$$

Furthermore, the log-likelihood function is obtained as:

$$\begin{aligned} \ln L(\rho, \boldsymbol{\beta}_0|\boldsymbol{\varepsilon}) &= \ln\left(\tfrac{1}{2\pi\sigma^2}\right)^{\frac{n}{2}} \exp\left[-\tfrac{(\mathbf{y}-\rho\mathbf{W}\mathbf{y}-\mathbf{A}\boldsymbol{\beta}_0)^T(\mathbf{y}-\rho\mathbf{W}\mathbf{y}-\mathbf{A}\boldsymbol{\beta}_0)}{2\sigma^2}\right] \\ &= -\tfrac{n}{2}\ln(2\pi) - \tfrac{n}{2}\ln\sigma^2 - \tfrac{(\mathbf{y}-\rho\mathbf{W}\mathbf{y}-\mathbf{A}\boldsymbol{\beta}_0)^T(\mathbf{y}-\rho\mathbf{W}\mathbf{y}-\mathbf{A}\boldsymbol{\beta}_0)}{2\sigma^2} \end{aligned} \tag{17}$$

A parameter estimation $\rho,\ \boldsymbol{\beta}_0$ is obtained by maximizing the log-likelihood function.

To obtain the MLE estimation of the parameters $\hat{\rho}$, the first derivative of Equation (17) for the parameters ρ was expressed as:

$$\begin{aligned} \tfrac{\partial \ln L(\rho,\boldsymbol{\beta}_0|\boldsymbol{\varepsilon})}{\partial \boldsymbol{\beta}_0} &= -\tfrac{(\mathbf{y}-\rho\mathbf{W}\mathbf{y}-\mathbf{A}\boldsymbol{\beta}_0)^T(-\mathbf{W}\mathbf{y})}{2\sigma^2} \\ &= \tfrac{(\mathbf{y}-\rho\mathbf{W}\mathbf{y}-\mathbf{A}\boldsymbol{\beta}_0)^T(\mathbf{W}\mathbf{y})}{2\sigma^2} \end{aligned} \tag{18}$$

$\left.\tfrac{\partial \ln L(\rho,\boldsymbol{\beta}_0|\boldsymbol{\varepsilon})}{\partial \rho}\right|_{\rho=\hat{\rho}} = 0$, this is further expressed as follows:

$$\frac{(\mathbf{y}-\rho\mathbf{W}\mathbf{y}-\mathbf{A}\boldsymbol{\beta}_0)^T(\mathbf{W}\mathbf{y})}{2\sigma^2} = 0 \tag{19}$$

In Equation (19), multiply by $2\sigma^2(\mathbf{W}\mathbf{y})^T$ to obtain:

$$(\mathbf{y}-\rho\mathbf{W}\mathbf{y}-\mathbf{A}\boldsymbol{\beta}_0)^T\left(\mathbf{W}\mathbf{y}(\mathbf{W}\mathbf{y})^T\right) = 0 \tag{20}$$

Multiply Equation (20) by $\left(\mathbf{W}\mathbf{y}(\mathbf{W}\mathbf{y})^T\right)^{-1}$ to obtain:

$$(\mathbf{y}-\rho\mathbf{W}\mathbf{y}-\mathbf{A}\boldsymbol{\beta}_0)^T = 0 \tag{21}$$

Transpose Equation (21) to obtain:

$$\mathbf{y}-\mathbf{A}\boldsymbol{\beta}_0 = \rho\mathbf{W}\mathbf{y} \tag{22}$$

In Equation (22), multiply both segments by $(\mathbf{W}\mathbf{y})^T$, thus obtaining:

$$(\mathbf{y}-\mathbf{A}\boldsymbol{\beta}_0)(\mathbf{W}\mathbf{y})^T = \rho\mathbf{W}\mathbf{y}(\mathbf{W}\mathbf{y})^T \tag{23}$$

From Equation (23), multiply both segments by $\left(\mathbf{W}\mathbf{y}(\mathbf{W}\mathbf{y})^T\right)^{-1}$ to further obtain:

$$(\mathbf{y}-\mathbf{A}\boldsymbol{\beta}_0)(\mathbf{W}\mathbf{y})^T\left(\mathbf{W}\mathbf{y}(\mathbf{W}\mathbf{y})^T\right)^{-1} = \rho\left(\mathbf{W}\mathbf{y}(\mathbf{W}\mathbf{y})^T\right)\left(\mathbf{W}\mathbf{y}(\mathbf{W}\mathbf{y})^T\right)^{-1} \tag{24}$$

$$\hat{\rho} = (\mathbf{y}-\mathbf{A}\boldsymbol{\beta}_0)(\mathbf{W}\mathbf{y})^T\left(\mathbf{W}\mathbf{y}(\mathbf{W}\mathbf{y})^T\right)^{-1} \tag{25}$$

Substitute the equation $\mathbf{A} = \mathbf{XZJ}$ into Equation (13), in order to determine $\hat{\rho}$ the following:

$$\hat{\rho} = (\mathbf{y}-(\mathbf{XZJ})\boldsymbol{\beta}_0)(\mathbf{W}\mathbf{y})^T\left(\mathbf{W}\mathbf{y}(\mathbf{W}\mathbf{y})^T\right)^{-1} \tag{26}$$

To obtain the MLE estimation of the parameters $\hat{\boldsymbol{\beta}}_0$, first determine the first derivative of Equation (17) for the parameters $\boldsymbol{\beta}_0$ as follows:

$$\begin{aligned} \tfrac{\partial \ln L(\rho,\boldsymbol{\beta}_0|\boldsymbol{\varepsilon})}{\partial \boldsymbol{\beta}_0} &= -\tfrac{(\mathbf{y}-\rho\mathbf{W}\mathbf{y}-\mathbf{A}\boldsymbol{\beta}_0)^T(-\mathbf{A})}{2\sigma^2} \\ &= \tfrac{(\mathbf{y}-\rho\mathbf{W}\mathbf{y}-\mathbf{A}\boldsymbol{\beta}_0)^T(\mathbf{A})}{2\sigma^2} \end{aligned} \tag{27}$$

$\frac{\partial \ln L(\rho,\boldsymbol{\beta}_0|\boldsymbol{\varepsilon})}{\partial \boldsymbol{\beta}_0}\Big|_{\boldsymbol{\beta}_0=\hat{\boldsymbol{\beta}}_0} = 0$. This leads to the equation below:

$$\frac{(\mathbf{y}-\rho\mathbf{W}\mathbf{y}-\mathbf{A}\boldsymbol{\beta}_0)^T\mathbf{A}}{2\sigma^2} = 0 \tag{28}$$

In Equation (28), multiply with $2\sigma^2\mathbf{A}^T$, in order to obtain:

$$(\mathbf{y}-\rho\mathbf{W}\mathbf{y}-\mathbf{A}\boldsymbol{\beta}_0)^T\mathbf{A}\mathbf{A}^T = 0 \tag{29}$$

Multiply Equation (29) by $\left(\mathbf{A}\mathbf{A}^T\right)^{-1}$ to obtain:

$$(\mathbf{y}-\rho\mathbf{W}\mathbf{y}-\mathbf{A}\boldsymbol{\beta}_0)^T = 0 \tag{30}$$

Transpose Equation (30), in order to obtain the expression below:

$$\mathbf{A}\boldsymbol{\beta}_0 = \mathbf{y}-\rho\mathbf{W}\mathbf{y} \tag{31}$$

In Equation (31), multiply both segments by $\mathbf{A}^T$ to obtain:

$$(\mathbf{A}\boldsymbol{\beta}_0)\mathbf{A}^T = (\mathbf{y}-\rho\mathbf{W}\mathbf{y})\mathbf{A}^T \tag{32}$$

From Equation (32), multiply both segments by $\left(\mathbf{A}\mathbf{A}^T\right)^{-1}$ to obtain the following expression:

$$\boldsymbol{\beta}_0\left(\mathbf{A}\mathbf{A}^T\right)\left(\mathbf{A}\mathbf{A}^T\right)^{-1} = (\mathbf{y}-\rho\mathbf{W}\mathbf{y})\mathbf{A}^T\left(\mathbf{A}\mathbf{A}^T\right)^{-1} \tag{33}$$

$$\hat{\boldsymbol{\beta}}_0 = (\mathbf{y}-\rho\mathbf{W}\mathbf{y})\mathbf{A}^T\left(\mathbf{A}\mathbf{A}^T\right)^{-1} \tag{34}$$

Substitute the equation $\mathbf{A} = \mathbf{XZJ}$ into Equation (13) and derive $\hat{\boldsymbol{\beta}}_0$ as follows:

$$\hat{\boldsymbol{\beta}}_0 = (\mathbf{y}-\rho\mathbf{W}\mathbf{y})(\mathbf{XZJ})^T\left((\mathbf{XZJ})(\mathbf{XZJ})^T\right)^{-1} \tag{35}$$

Based on the estimated parameter $\hat{\boldsymbol{\beta}}_0$ in Equation (35), the value $\boldsymbol{\beta}$ can be obtained by substituting into Equation (11):

$$\boldsymbol{\beta}=\mathbf{ZJ}\left((\mathbf{y}-\rho\mathbf{W}\mathbf{y})(\mathbf{XZJ})^T\left((\mathbf{XZJ})(\mathbf{XZJ})^T\right)^{-1}\right) \tag{36}$$

3. Real Data Application

3.1. Data Description

In this research, secondary data from 13 climate observation stations in West Java were utilized. These data were sourced from the Meteorology, Climatology, and Geophysics Agency (BMKG), while climate variable data were extracted from the National Aeronautics and Space Administration Prediction of Worldwide Energy Resources (NASA POWER) satellite observations. The climate variable dataset included rainfall, air temperature, humidity, solar irradiation, wind speed, and surface pressure shown on Table 1.

Table 1. Climate variable data at 13 climate observation stations in West Java.

No.	Locations	Latitude	Longitude	Rainfall (mm)	Air Temperature (°C)	Humidity (%)	Solar Irradiation (W/m^2)	Wind Speed (m/s)	Surface Pressure (kPa)
1	Balitpa Sukamandi	−6.3	107.65	186.36	25.3	83.45	415.2	1.76	97.86
2	Lanud Atang Sanjaya Semplak	−6.9	106.77	200.74	23.72	87.25	411.23	1.71	95.52
3	LPHP Tasikmalaya	−7.28	108.16	228.2	23.68	89.15	398.29	2.1	96.46
4	SMPK Cirebon	−6.72	108.58	189.71	27.7	78.58	418.72	3.67	100.86
5	SMPK Maranginan Sukabumi	−7.25	106.25	191.42	25.79	84.61	415.46	3.12	98.84
6	SMPK Nariewattie	−7.25	108	194.57	22.59	87.85	398.29	1.57	93.62
7	SMPK Pacet Cianjur	−6.73	107	176.28	24.7	85.19	415.2	1.46	96.82
8	SMPK Pasir Sarongge	−6.75	107	176.28	24.7	85.19	415.2	1.46	96.82
9	Stage of Bandung	−6.92	107.6	203.29	21.41	88.29	415.2	1.51	90.93
10	Stage of Lembang	−6.83	107.62	203.29	21.41	88.29	415.2	1.51	90.93
11	Staklim Darmaga	−6.55	106.75	176.28	24.7	85.19	411.23	1.46	96.82
12	Stamet Citeko Bogor	−6.7	106.93	176.28	24.7	85.19	411.23	1.46	96.82
13	Stamet Jatiwangi	−6.75	108.27	181.08	26.45	80.97	418.72	2.49	99.66

3.2. RShiny Web Application for SAR-X Model

At this stage, an R script was developed to process the data using the SAR-X model through the RShiny web application.

A. The process of building an R script for the SAR-X model

The SAR-X modeling process, employing the Casetti model approach, entailed the following steps:

1. Importing the climate data used for the SAR-X modeling, encompassing 13 climate observation stations in the West Java region.
2. Constructing vectors and matrices based on the climate data, including:
    a. Vector **y**: defines the rainfall variable at each location.
    b. Matrix **X**: represents the exogenous variables, such as air temperature, humidity, solar irradiation, wind speed, and surface pressure.
    c. Matrix **Z**: consists of location coordinate entries in latitude and longitude.
    d. Matrix **J**: identity matrix with the size of as many as five exogenous variables, according to matrix **X**.
    e. Matrix **W**: the result of calculating the inverse distance weight matrix using the equation with input location coordinates (latitude and longitude).
    f. Kronecker **Z**: the expression obtained from the multiplication of the kronecker with the identity matrix of the five exogenous variables $(\mathbf{Z} \otimes \mathbf{I}_k)$
    g. Matrix **A**: the product of matrix **X**, **Z**, and **J**
3. The Moran Index calculation using function "moran.test" and Moran Scatterplot using function "moran.plot".

4. The calculation of parameter estimation $\hat{\rho}$ and $\hat{\beta}_0$, obtaining the prediction results $\hat{\mathbf{y}}$, absolute error, and MAPE of the SAR-X model prediction with the Casetti model approach.
5. The SAR-X model prediction data with the Casetti model approach in the form of $\hat{\mathbf{y}}$

B. Creating and publishing the RShiny web application with the developed script.

At this stage, the R script explicitly built for the SAR-X model was transformed into an RShiny web application following these steps:

1. Installing packages and call libraries, specifically "shiny" and "shinythemes", to set up RShiny.
2. Creating a User Interface (UI) and Server for the Web Application UI scripts managed the appearance of the web, incorporating headers, images, panel tabs, and more. Furthermore, the previously crafted R script for the SAR-X model was integrated into the server script. Running the application involved clicking "Run App." Successful execution prompted progression, while errors in the console necessitated troubleshooting.
3. Publishing the RShiny Web Application

At this stage, the designed application was published on the https://www.shinyapps.io platform, accessed on 5 July 2023. The account creation on the site was followed by token activation. The provided token was copied and inserted into RStudio. The application could be published by clicking the designated icon.

3.3. Calculation Result of Inverse Distance Weight Matrix

The inverse distance weight was computed by taking into account the actual distances between each location. The standardized inverse distance weight matrix for the SAR-X model was then obtained using Equation (2), which produced the following:

$$W = \begin{pmatrix}
0 & 0.049832 & 0.046317 & 0.054288 & 0.019748 & 0.055151 & 0.093068 & 0.090447 & 0.146109 & 0.200602 & 0.06479 & 0.083328 & 0.096319 \\
0.015477 & 0 & 0.008455 & 0.005307 & 0.044687 & 0.010736 & 0.214639 & 0.232858 & 0.025472 & 0.024137 & 0.14286 & 0.267645 & 0.007726 \\
0.016001 & 0.009405 & 0 & 0.039857 & 0.005352 & 0.736974 & 0.01185 & 0.012007 & 0.044065 & 0.039526 & 0.007747 & 0.010561 & 0.066655 \\
0.050697 & 0.015956 & 0.107736 & 0 & 0.009246 & 0.085519 & 0.021146 & 0.021139 & 0.05277 & 0.056539 & 0.015629 & 0.019388 & 0.544235 \\
0.034948 & 0.254618 & 0.027416 & 0.017521 & 0 & 0.032666 & 0.12011 & 0.123126 & 0.051796 & 0.048721 & 0.135189 & 0.130788 & 0.023102 \\
0.018078 & 0.01133 & 0.699231 & 0.030017 & 0.00605 & 0 & 0.014586 & 0.014824 & 0.068909 & 0.057761 & 0.009028 & 0.012802 & 0.057385 \\
0.000609 & 0.004519 & 0.000224 & 0.000148 & 0.000444 & 0.000291 & 0 & 0.924044 & 0.000933 & 0.000937 & 0.003895 & 0.063727 & 0.000229 \\
0.0006 & 0.00497 & 0.00023 & 0.00015 & 0.000461 & 0.0003 & 0.936838 & 0 & 0.000964 & 0.000959 & 0.003656 & 0.05064 & 0.000232 \\
0.018523 & 0.010397 & 0.01617 & 0.007164 & 0.003711 & 0.026651 & 0.018093 & 0.018428 & 0 & 0.843116 & 0.008339 & 0.014411 & 0.014999 \\
0.025362 & 0.009825 & 0.014464 & 0.007654 & 0.003481 & 0.022278 & 0.018121 & 0.018288 & 0.84081 & 0 & 0.008556 & 0.014497 & 0.016663 \\
0.021581 & 0.153208 & 0.007469 & 0.005574 & 0.025445 & 0.009174 & 0.198412 & 0.1837 & 0.02191 & 0.022542 & 0 & 0.342974 & 0.008011 \\
0.004212 & 0.043556 & 0.001545 & 0.001049 & 0.003735 & 0.001974 & 0.492634 & 0.386119 & 0.005746 & 0.005796 & 0.052045 & 0 & 0.001589 \\
0.065939 & 0.01703 & 0.132081 & 0.398967 & 0.008937 & 0.119851 & 0.023988 & 0.023994 & 0.080996 & 0.09023 & 0.016465 & 0.021523 & 0
\end{pmatrix}$$

3.4. Calculation Result of Moran's Index and Scatterplot Moran

The calculation of the Moran Index was employed to assess the existence of spatial autocorrelation among the observation locations. The Moran Index for each climate variable was calculated using Equation (4). The results of the Moran index calculations are shown on Table 2.

Aside from the computation of the Moran Index on Table 2, a Moran Scatterplot was also utilized to visualize the overall clustering tendency and distinctive attributes of each region. This visual representation took the form of a four-quadrant graph for each unit of analysis. The four quadrants showed potential groupings, bounded by mean and average lines. Areas were considered to have high attributes when their values exceeded the average, while values below the average indicated low characteristics. The complete results of the Moran Scatterplot for each climate variable can be seen in Figure 1.

Table 2. Spatial autocorrelation test using Moran's Index.

No.	Climate Variable	p-Value	Description
1	**y** (Rainfall)	0.0168	There is spatial autocorrelation
2	$\mathbf{X}_1$ (Air Temperature)	0.0061	There is spatial autocorrelation
3	$\mathbf{X}_2$ (Humidity)	0.0163	There is spatial autocorrelation
4	$\mathbf{X}_3$ (Solar Irradiation)	0.0013	There is spatial autocorrelation
5	$\mathbf{X}_4$ (Wind Speed)	0.0487	There is spatial autocorrelation
6	$\mathbf{X}_5$ (Surface Pressure)	0.0044	There is spatial autocorrelation

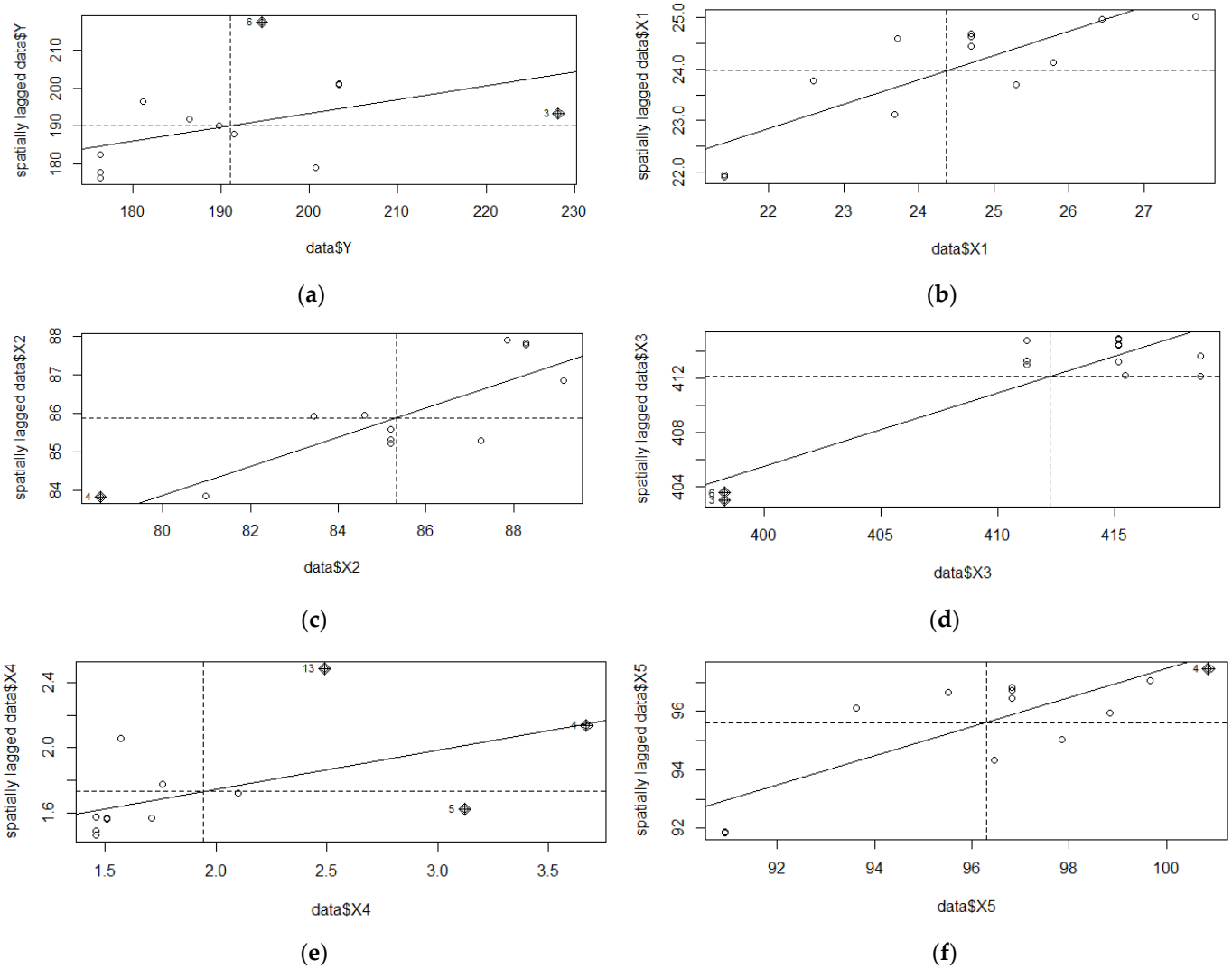

Figure 1. Moran's scatterplot of climate variables: (**a**) rainfall, (**b**) air temperature, (**c**) humidity, (**d**) solar ir-radiation, (**e**) wind speed, and (**f**) surface pressure.

3.5. Prediction Result of SAR Model

The estimation of the prediction parameters $\hat{\rho}$ and $\hat{\boldsymbol{\beta}}$ in the SAR model was conducted using R version 4.2.2. An estimated $\hat{\rho}$ value of 0.744 was obtained, indicating spatial lag dependence. This signified the influence of adjacent locations within the West Java region on the rainfall prediction data. The results of the calculation of the parameter estimate for $\hat{\boldsymbol{\beta}}$ are shown in Table 3.

Table 3. Parameter estimated value $\hat{\boldsymbol{\beta}}$.

No.	$\hat{\boldsymbol{\beta}}$	Parameter Estimated Value
1	β_1	−89.56
2	β_2	−12.21
3	β_3	−0.63
4	β_4	27.50
5	β_5	36.49

The SAR model equation for each location is presented and can be found in Appendix A. The predictions of rainfall and absolute errors at each location are shown in Table 4.

Table 4. Prediction results and error prediction of SAR model.

No.	Locations	y	$\hat{y}$	Absolute Error
1	Balitpa Sukamandi	186.36	214.49	15.09
2	Lanud Atang Sanjaya Semplak	200.74	215.98	7.59
3	LPHP Tasikmalaya	228.20	260.09	13.98
4	SMPK Cirebon	189.71	217.49	14.64
5	SMPK Maranginan Sukabumi	191.42	226.58	18.37
6	SMPK Nariewattie	194.57	273.16	40.39
7	SMPK Pacet Cianjur	176.28	189.40	7.44
8	SMPK Pasir Sarongge	176.28	189.41	7.45
9	Stage of Bandung	203.29	250.93	23.44
10	Stage of Lembang	203.29	250.81	23.38
11	Staklim Darmaga	176.28	196.39	11.41
12	Stamet Citeko Bogor	176.28	192.96	9.46
13	Stamet Jatiwangi	181.08	228.85	26.38

Based on the results of the absolute error calculation in Table 4, the MAPE (Mean Absolute Percentage Error) value for prediction using the SAR model amounted to 16.85%. According to Lewis (1982) in [40], the prediction accuracy level is accurate, as the MAPE was less than 20%.

3.6. Prediction Result of SAR-X Model

The estimation of the prediction parameters $\hat{\rho}$ and $\hat{\boldsymbol{\beta}}_0$ in the SAR-X model was conducted using R software through a web application powered by RShiny. An estimated $\hat{\rho}$ value of 1.001973 was obtained, indicating spatial lag dependence. This signified the influence of adjacent locations within the West Java region on the rainfall prediction data. The results of the parameter estimate calculation of $\hat{\boldsymbol{\beta}}_0$ for each $\hat{\boldsymbol{\beta}}_{latitude}$ and $\hat{\boldsymbol{\beta}}_{longitude}$ are shown in Table 5.

Table 5. Parameter estimated value $\hat{\beta}_0$ for each $\hat{\beta}_{latitude}$ and $\hat{\beta}_{longitude}$.

No.	$\hat{\beta}_0$	Parameter Estimated Value
1	$\hat{\beta}_{latitude(x_1)}$	−539.33
2	$\hat{\beta}_{longitude(x_1)}$	−96.53
3	$\hat{\beta}_{latitude(x_2)}$	2.93
4	$\hat{\beta}_{longitude(x_2)}$	139.34
5	$\hat{\beta}_{latitude(x_3)}$	207.11
6	$\hat{\beta}_{longitude(x_3)}$	−33.57
7	$\hat{\beta}_{latitude(x_4)}$	−5.94
8	$\hat{\beta}_{longitude(x_4)}$	0.17
9	$\hat{\beta}_{latitude(x_5)}$	8.96
10	$\hat{\beta}_{longitude(x_5)}$	12.86

Based on the estimated value of $\hat{\beta}_0$ in Table 5, the value of $\hat{\beta}$ was determined using Equation (38). The calculated values of $\hat{\beta}$ are shown in Table 6.

Table 6. Parameter estimated value of $\hat{\beta}$.

No.	Locations	Parameter Estimated Value of $\hat{\beta}$				
		$\hat{\beta}_1$	$\hat{\beta}_2$	$\hat{\beta}_3$	$\hat{\beta}_4$	$\hat{\beta}_5$
1	Balitpa Sukamandi	−215.93	−45.51	58.56	−21.52	−0.73
2	Lanud Atang Sanjaya Semplak	−31.14	−116.44	−2.56	120.40	43.66
3	LPHP Tasikmalaya	0.16	−20.48	−42.76	29.06	16.71
4	SMPK Cirebon	86.59	3.91	−112.28	−1.67	24.16
5	SMPK Maranginan Sukabumi	80.12	−0.91	38.00	−0.32	11.79
6	SMPK Nariewattie	137.49	36.36	14.27	−49.03	−1.14
7	SMPK Pacet Cianjur	32.06	5.04	−1.21	71.15	24.35
8	SMPK Pasir Sarongge	−1.75	343.87	20.79	20.24	−12.06
9	Stage of Bandung	−4.98	68.96	−17.38	−1.40	6.13
10	Stage of Lembang	−55.57	−2.87	48.79	12.41	8.65
11	Staklim Darmaga	295.90	−58.45	16.20	−30.12	−1.05
12	Stamet Citeko Bogor	60.51	−134.81	−1.27	−50.76	29.39
13	Stamet Jatiwangi	−2.62	285.08	18.01	−1.64	−5.17

The SAR-X model equation for each location can be found in Appendix B. The predictions of the rainfall and corresponding errors at each location are shown in Table 7.

Based on the results of the absolute error calculation in Table 7, the MAPE value for prediction using the SAR-X model amounted to 1.95%. According to Lewis (1982) in [40], the prediction accuracy level is very accurate, as the MAPE value was less than 10%.

Table 7. Prediction results and absolute error prediction of SAR-X Model.

No.	Locations	y	$\hat{y}$	Absolute Error
1	Balitpa Sukamandi	186.36	189.49	1.68
2	Lanud Atang Sanjaya Semplak	200.74	200.78	0.02
3	LPHP Tasikmalaya	228.20	222.30	2.59
4	SMPK Cirebon	189.71	190.80	0.57
5	SMPK Maranginan Sukabumi	191.42	193.36	1.01
6	SMPK Nariewattie	194.57	202.01	3.82
7	SMPK Pacet Cianjur	176.28	175.13	0.65
8	SMPK Pasir Sarongge	176.28	176.62	0.19
9	Stage of Bandung	203.29	193.78	4.68
10	Stage of Lembang	203.29	210.81	3.70
11	Staklim Darmaga	176.28	171.90	2.48
12	Stamet Citeko Bogor	176.28	179.17	1.64
13	Stamet Jatiwangi	181.08	176.87	2.32

3.7. Cross-Validation

In this research, for a cross-validation study, the data collection stage was carried out through a parameter selection process in the form of climate variable data. Those used were rainfall, solar irradiance, and wind speed in the West Java region, consisting of 11 regencies/cities shown on Table 8.

Table 8. Climate variable data from 11 regencies/cities in West Java.

No.	Locations	Latitude	Longitude	Rainfall (mm)	Solar Irradiation (W/m^2)	Wind Speed (m/s)
1	Bandung City	−6.91486	107.6082	203.29	415.2	1.511
2	Bekasi City	−6.24159	106.9924	172.32	411.2	2.492
3	Cirebon City	−6.73725	108.5507	189.71	418.7	3.674
4	Sukabumi City	−6.9237	106.9287	200.74	411.2	1.706
5	Tasikmalaya City	−7.31956	108.203	228.2	398.3	2.099
6	Pangandaran Regency	−7.61506	108.4988	210.14	1.816	398.3
7	Bogor Regency	−6.59504	106.8166	176.28	411.2	1.456
8	Majalengka Regency	−6.83638	108.2274	194.57	418.7	1.575
9	Indramayu Regency	−6.32758	108.3249	181.08	418.7	2.495
10	Purwakarta Regency	−6.53868	107.4499	186.36	415.2	1.76
11	Kuningan Regency	−7.01381	108.5701	184.64	398.3	1.781

An estimated $\hat{\rho}$ value of 0.8055492 was obtained, indicating spatial lag dependence. This signified the influence of adjacent locations within the West Java region on the rainfall prediction data. The results of the parameter estimate calculations of $\hat{\beta}_0$ for each $\hat{\beta}_{latitude}$ and $\hat{\beta}_{longitude}$ are shown in Table 9.

The results of calculating the estimated value of $\hat{\beta}$ are shown in Table 10.

The results of predictions of the rainfall and absolute errors at each location are shown in Table 11.

Based on the results of the absolute error calculation in Table 11, the MAPE value for prediction with the SAR-X model in the cross-validation dataset was 7.09% and the prediction accuracy level was very accurate, as the MAPE value was less than 10%.

Table 9. Parameter estimated value $\hat{\beta}_0$ for cross-validation dataset.

No.	$\hat{\beta}_0$	Parameter Estimated Value
1	$\hat{\beta}_{latitude(x_1)}$	−0.08
2	$\hat{\beta}_{longitude(x_1)}$	4.04
3	$\hat{\beta}_{latitude(x_2)}$	−0.01
4	$\hat{\beta}_{longitude(x_2)}$	0.35

Table 10. Parameter estimated value of $\hat{\beta}$ for cross-validation dataset.

No.	Locations	Parameter Estimated Value of $\hat{\beta}$	
		$\hat{\beta}_1$	$\hat{\beta}_2$
1	Bandung City	0.11	−0.06
2	Bekasi City	2.72	0.08
3	Cirebon City	0.03	3.88
4	Sukabumi City	5.48	0.10
5	Tasikmalaya City	0.08	3.26
6	Pangandaran Regency	3.79	0.03
7	Bogor Regency	0.12	5.51
8	Majalengka Regency	2.48	0.07
9	Indramayu Regency	0.16	4.32
10	Purwakarta Regency	1.14	0.12
11	Kuningan Regency	0.20	2.59

Table 11. Prediction results and MAPE Prediction of SAR-X Model for cross-validation dataset.

No.	Locations	y	$\hat{y}$	Absolute Error
1	Bandung City	203.29	206.08	2.79
2	Bekasi City	172.32	177.63	5.31
3	Cirebon City	189.71	203.23	13.52
4	Sukabumi City	200.74	201.40	0.66
5	Tasikmalaya City	228.20	223.60	4.60
6	Pangandaran Regency	210.14	140.21	69.93
7	Bogor Regency	176.28	191.01	14.73
8	Majalengka Regency	194.57	203.28	8.71
9	Indramayu Regency	181.08	183.86	2.78
10	Purwakarta Regency	186.36	190.22	3.86
11	Kuningan Regency	184.64	211.11	26.47

4. Discussion

The procedure for predicting rainfall in West Java, utilizing the SAR-X model with the Casetti Model approach, was conducted based on data from 13 climate observation

stations. The entire process was carried out within the RStudio software environment, leveraging the capabilities of the RShiny web application. The R script constructed for this purpose encompassed various stages of the SAR-X modeling procedure, ranging from data import, vector, matrix construction, Moran index, Moran scatterplot calculation, parameter estimation, prediction result calculation, and MAPE assessment to the publication of the RShiny web application. It should be noted that the execution time of the script ranged from 1 to 5 min. The source code is stored in the GitHub directory and the link is included in Appendix C, which could be valuable for facilitating the replication and verification of the model and its results by other researchers [41,42].

The result of the Moran index calculation, presented in Table 2, showed a positive spatial autocorrelation across the 13 observation stations within the West Java region. In addition, it concurred with the descriptive analysis, indicating that the areas exhibiting high rainfall tended to be situated in proximity to other high-rainfall areas, and vice versa. The results of the identification, parameter estimation, and prediction of rainfall, involving five other climate variable factors in Tables 4 and 7, showed that the MAPE value of the SAR-X model prediction results was smaller than the MAPE of the SAR model, with the calculation of the rainfall prediction providing very high results based on the MAPE value of 1.95%. This shows that the prediction of rainfall using NASA POWER data from 13 observation stations in the West Java region using the SAR-X model was better than prediction with the SAR model, because the SAR-X model obtained $\hat{\boldsymbol{\beta}}$ parameters that varied for each exogenous variable at each location. This research aligned with the discovery of Hermawan [28], highlighting the influential role of five climate variable factors in shaping rainfall patterns, namely air temperature, humidity, solar irradiation, wind speed, and surface pressure.

5. Conclusions

In conclusion, the SAR-X model using Casetti's approach was applied to analyze the rainfall data and climate variables in West Java, utilizing information from 13 climate observation stations. These data showed a positive spatial autocorrelation among different regions. The results highlighted the remarkable accuracy of the prediction outcomes obtained through the SAR-X model at each observation location. This accuracy was attributed to the distinct estimated parameter values assigned to each climate variable, contributing to the high precision of the prediction results.

The summary of this research underscored that the level of rainfall in each region, based on the data from 13 climate observation stations in West Java, was significantly influenced by five other climate variable factors. It should be noted that these factors collectively exhibited a positive spatial autocorrelation across various areas. Therefore, the recommendation for relevant institutions engaged in rainfall prediction is to thoroughly consider the diverse aspects of climate variables. This approach enables a comprehensive understanding of how each climate variable exerts its influence within distinct locations.

6. Patents

Granted Copy Right: Copy Right for Computer Program, number 000484465.

Entitled "Application of RShiny Program for SAR-X with Casetti Model Approach to Climate Data in West Java", Ministry of Law and Human Rights of the Republic of Indonesia (Falah, A. N., Ruchjana, B. N., Abdullah, A. S., Rejito, J.), 2023. https://annisanurfalah.shinyapps.io/SAR-X-Model/, accessed on 5 July 2023.

Author Contributions: Conceptualization, A.N.F., B.N.R. and A.S.A.; methodology, A.N.F.; software, A.N.F.; validation, A.N.F. and B.N.R.; formal analysis, A.N.F., B.N.R. and A.S.A.; investigation, A.S.A. and J.R.; resources, B.N.R.; data curation A.N.F.; writing—original draft preparation, A.N.F.; writing—review and editing, A.N.F., B.N.R., A.S.A. and J.R.; supervision, B.N.R., A.S.A. and J.R.; project administration A.N.F. and B.N.R.; funding acquisition, B.N.R. All authors have read and agreed to the published version of the manuscript.

Funding: The APC was funded by Academic Leadership Grant Universitas Padjadjaran with contract number: 1549/UN6.3.1/PT.00/2023.

Data Availability Statement: Not applicable.

Acknowledgments: The authors thank to the Rector, Directorate of Research and Community Service (DRPM), and Studies Center of Modeling and Computation Faculty of Mathematics and Natural Sciences, Universitas Padjadjaran. The authors thank to the Commission Developing Country (CDC)—International Mathematical Union (IMU) Breakout Graduate Fellowship 2020–2023, Academic Leadership Grant (ALG) with contract number 1549/UN6.3.1/PT.00/2023, and International Consortium RISE_SMA project 2019–2024.

Conflicts of Interest: The authors declare no conflict of interest.

Appendix A

- SAR model for predicting rainfall in Balitpa Sukamandi:

$$\hat{y}_{(s_1)} = 0.744\sum_{i=1}^{13} w_{1i}y_{(s_i)} - 89.56X_1 - 12.21X_2 - 0.63X_3 + 27.50X_4 + 36.49X_5$$

- SAR model for predicting rainfall in Lanud Atang Sanjaya Semplak:

$$\hat{y}_{(s_2)} = 0.744\sum_{i=1}^{13} w_{2i}y_{(s_i)} - 89.56X_1 - 12.21X_2 - 0.63X_3 + 27.50X_4 + 36.49X_5$$

- SAR model for predicting rainfall in LPHP Tasikmalaya:

$$\hat{y}_{(s_3)} = 0.744\sum_{i=1}^{13} w_{3i}y_{(s_i)} - 89.56X_1 - 12.21X_2 - 0.63X_3 + 27.50X_4 + 36.49X_5$$

- SAR model for predicting rainfall in SMPK Cirebon:

$$\hat{y}_{(s_4)} = 0.744\sum_{i=1}^{13} w_{4i}y_{(s_i)} - 89.56X_1 - 12.21X_2 - 0.63X_3 + 27.50X_4 + 36.49X_5$$

- SAR model for predicting rainfall in SMPK Maranginan Sukabumi:

$$\hat{y}_{(s_5)} = 0.744\sum_{i=1}^{13} w_{5i}y_{(s_i)} - 89.56X_1 - 12.21X_2 - 0.63X_3 + 27.50X_4 + 36.49X_5$$

- SAR model for predicting rainfall in SMPK Nariewattie:

$$\hat{y}_{(s_6)} = 0.744\sum_{i=1}^{13} w_{6i}y_{(s_i)} - 89.56X_1 - 12.21X_2 - 0.63X_3 + 27.50X_4 + 36.49X_5$$

- SAR model for predicting rainfall in SMPK Pacet Cianjur:

$$\hat{y}_{(7)} = 0.744\sum_{i=1}^{13} w_{7i}y_{(s_i)} - 89.56X_1 - 12.21X_2 - 0.63X_3 + 27.50X_4 + 36.49X_5$$

- SAR model for predicting rainfall in SMPK Pasir Sarongge:

$$\hat{y}_{(s_8)} = 0.744\sum_{i=1}^{13} w_{8i}y_{(s_i)} - 89.56X_1 - 12.21X_2 - 0.63X_3 + 27.50X_4 + 36.49X_5$$

- SAR model for predicting rainfall in Stage of Bandung:

$$\hat{y}_{(s_9)} = 0.744\sum_{i=1}^{13} w_{9i}y_{(s_i)} - 89.56X_1 - 12.21X_2 - 0.63X_3 + 27.50X_4 + 36.49X_5$$

- SAR model for predicting rainfall in Stage of Lembang:

$$\hat{y}_{(10)} = 0.744\ \sum_{i=1}^{13} w_{10i}y_{(s_i)} - 89.56X_1 - 12.21X_2 - 0.63X_3 + 27.50X_4 + 36.49X_5$$

- SAR model for predicting rainfall in Staklim Darmaga:

$$\hat{y}_{(s_{11})} = 0.744\ \sum_{i=1}^{13} w_{11i}y_{(s_i)} - 89.56X_1 - 12.21X_2 - 0.63X_3 + 27.50X_4 + 36.49X_5$$

- SAR model for predicting rainfall in Stamet Citeko Bogor:

$$\hat{y}_{(s_{12})} = 0.744\sum_{i=1}^{13} w_{12i}y_{(s_i)} - 89.56X_1 - 12.21X_2 - 0.63X_3 + 27.50X_4 + 36.49X_5$$

- SAR model for predicting rainfall in Stamet Jatiwangi:

$$\hat{y}_{(s_{13})} = 0.744\sum_{i=1}^{13} w_{13i}y_{(s_i)} - 89.56X_1 - 12.21X_2 - 0.63X_3 + 27.50X_4 + 36.49X_5$$

Appendix B

- SAR-X model for predicting rainfall in Balitpa Sukamandi:

$$\hat{y}_{(s_1)} = 1.001973\sum_{i=1}^{13} w_{1i}y_{(s_i)} - 215.93X_1 - 45.51X_2 + 58.56X_3 - 21.52X_4 - 0.73X_5$$

- SAR-X model for predicting rainfall in Lanud Atang Sanjaya Semplak:

$$\hat{y}_{(s_2)} = 1.001973\sum_{i=1}^{13} w_{2i}y_{(s_i)} - 31.14X_1 - 116.44X_2 - 2.56X_3 + 120.40X_4 + 43.66X_5$$

- SAR-X model for predicting rainfall in LPHP Tasikmalaya:

$$\hat{y}_{(s_3)} = 1.001973\sum_{i=1}^{13} w_{3i}y_{(s_i)} + 0.16X_1 - 20.48X_2 - 42.76X_3 + 29.06X_4 + 16.71X_5$$

- SAR-X model for predicting rainfall in SMPK Cirebon:

$$\hat{y}_{(s_4)} = 1.001973\sum_{i=1}^{13} w_{4i}y_{(s_i)} + 86.59X_1 + 3.91X_2 - 112.28X_3 - 1.67X_4 + 24.16X_5$$

- SAR-X model for predicting rainfall in SMPK Maranginan Sukabumi:

$$\hat{y}_{(s_5)} = 1.001973\sum_{i=1}^{13} w_{5i}y_{(s_i)} + 80.12X_1 - 0.91X_2 + 38.00X_3 - 0.32X_4 + 11.79X_5$$

- SAR-X model for predicting rainfall in SMPK Nariewattie:

$$\hat{y}_{(s_6)} = 1.001973\sum_{i=1}^{13} w_{6i}y_{(s_i)} + 137.49X_1 + 36.36X_2 + 14.27X_3 - 49.03X_4 - 1.14X_5$$

- SAR-X model for predicting rainfall in SMPK Pacet Cianjur:

$$\hat{y}_{(s_7)} = 1.001973 \sum_{i=1}^{13} w_{7i} y_{(s_i)} + 32.06X_1 + 5.04X_2 - 1.21X_3 + 71.15X_4 + 24.35X_5$$

- SAR-X model for predicting rainfall in SMPK Pasir Sarongge:

$$\hat{y}_{(s_8)} = 1.001973 \sum_{i=1}^{13} w_{8i} y_{(s_i)} - 1.75X_1 + 343.87X_2 + 20.79X_3 + 20.24X_4 - 12.06X_5$$

- SAR-X model for predicting rainfall in Stage of Bandung:

$$\hat{y}_{(s_9)} = 1.001973 \sum_{i=1}^{13} w_{9i} y_{(s_i)} - 4.98X_1 + 68.96X_2 - 17.38X_3 - 1.40X_4 + 6.13X_5$$

- SAR-X model for predicting rainfall in Stage of Lembang:

$$\hat{y}_{(s_{10})} = 1.001973 \sum_{i=1}^{13} w_{10i} y_{(s_i)} - 55.57X_1 - 2.87X_2 + 48.79X_3 + 12.41X_4 + 8.65X_5$$

- SAR-X model for predicting rainfall in Staklim Darmaga:

$$\hat{y}_{(s_{11})} = 1.001973 \sum_{i=1}^{13} w_{11i} y_{(s_i)} + 295.90X_1 - 58.45X_2 + 16.20X_3 - 30.12X_4 - 1.05X_5$$

- SAR-X model for predicting rainfall in Stamet Citeko Bogor:

$$\hat{y}_{(s_{12})} = 1.001973 \sum_{i=1}^{13} w_{12i} y_{(s_i)} + 60.51X_1 - 134.81X_2 - 1.27X_3 - 50.76X_4 + 29.39X_5$$

- SAR-X model for predicting rainfall in Stamet Jatiwangi:

$$\hat{y}_{(s_{13})} = 1.001973 \sum_{i=1}^{13} w_{13i} y_{(s_i)} - 2.62X_1 + 285.08X_2 + 18.01X_3 - 1.64X_4 - 5.17X_5$$

Appendix C

The source code is stored in the GitHub directory and can be accessed at the following link: https://github.com/annisanurfalah02/SAR-X-Model, accessed on 15 August 2023.

References

1. Shoji, T.; Kitaura, H. Statistical and geostatistical analysis of rainfall in central Japan. *Comput. Geosci.* **2006**, *32*, 1007–1024. [CrossRef]
2. Bostan, P.A.; Zuhal, A. *Exploring The Mean Annual Precipitation and Temperature Values over Turkey by Using Environmental Variables*; University of Applied Sciences: Stuttgart, Germany, 2006; pp. 1–6.
3. Cannarozzo, M.; Noto, L.V.; Viola, F. Spatial distribution of rainfall trends in Sicily (1921–2000). *Phys. Chem. Earth* **2006**, *31*, 1201–1211. [CrossRef]
4. Diodato, N.; Tartari, G.; Bellocchi, G. Geospatial Rainfall Modelling at Eastern Nepalese Highland from Ground Environmental Data. *Water Resour. Manag.* **2010**, *24*, 2703–2720. [CrossRef]
5. Basistha, A.; Arya, D.S.; Goel, N.K. Spatial distribution of rainfall in Indian Himalayas—A case study of Uttarakhand Region. *Water Resour. Manag.* **2008**, *22*, 1325–1346. [CrossRef]
6. Yilmaz, B.; Harmancioglu, N.B. An Indicator Based Assessment for Water Resources Management in Gediz River Basin, Turkey. *Water Resour. Manag.* **2010**, *24*, 4359–4379. [CrossRef]
7. Zimit, A.Y.; Jibril, M.M.; Azimi, M.S.; Abba, S.I. Hybrid predictive based control of precipitation in a water-scarce region: A focus on the application of intelligent learning for green irrigation in agriculture sector. *J. Saudi Soc. Agric. Sci.* **2023**. [CrossRef]
8. Hussain, A.; Jadoon, K.Z.; Rahman, K.U.; Shang, S.; Shahid, M.; Ejaz, N.; Khan, H. Analyzing the impact of drought on agriculture: Evidence from Pakistan using standardized precipitation evapotranspiration index. *Nat. Hazards* **2023**, *115*, 389–408. [CrossRef]

9. Ali, U.; Jing, W.; Zhu, J.; Omarkhanova, Z.; Fahad, S.; Nurgazina, Z.; Khan, Z.A. Climate change impacts on agriculture sector: A case study of Pakistan. *Cienc. Rural* **2021**, *51*, e20200110. [CrossRef]
10. Duncan, J.M.A.; Biggs, E.M.; Dash, J.; Atkinson, P.M. Spatio-temporal trends in precipitation and their implications for water resources management in climate-sensitive Nepal. *Appl. Geogr.* **2013**, *43*, 138–146. [CrossRef]
11. Hartmann, H.; Snow, J.A.; Su, B.; Jiang, T. Seasonal predictions of precipitation in the Aksu-Tarim River basin for improved water resources management. *Glob. Planet. Chang.* **2016**, *147*, 86–96. [CrossRef]
12. Li, L.; Hong, Y.; Wang, J.; Adler, R.F.; Policelli, F.S.; Habib, S.; Irwn, D.; Korme, T.; Okello, L. Evaluation of the real-time TRMM-based multi-satellite precipitation analysis for an operational flood prediction system in Nzoia Basin, Lake Victoria, Africa. *Nat. Hazards* **2009**, *50*, 109–123. [CrossRef]
13. Sharma, S.; Khadka, N.; Hamal, K.; Baniya, B.; Luintel, N.; Joshi, B.B. Spatial and Temporal Analysis of Precipitation and Its Extremities in Seven Provinces of Nepal. *Appl. Ecol. Environ. Sci.* **2020**, *8*, 64–73.
14. Wei, N.; Sun, X.; Bi, X.; Wang, J.M.; Li, X. The spatial characteristics of precipitation and water-logging disaster during rainy season for urban planning in Xi'an. *Indoor Built Environ.* **2019**, *28*, 1263–1271. [CrossRef]
15. Cheng, L.; Aghakouchak, A. Nonstationary precipitation intensity-duration-frequency curves for infrastructure design in a changing climate. *Sci. Rep.* **2014**, *4*, 7093. [CrossRef] [PubMed]
16. Rosenberg, E.A.; Keys, P.W.; Booth, D.B.; Hartley, D.; Burkey, J.; Steinemann, A.C.; Lettenmaier, D.P. Precipitation extremes and the impacts of climate change on stormwater infrastructure in Washington State. *Clim. Chang.* **2010**, *102*, 319–349. [CrossRef]
17. Nissen, K.M.; Ulbrich, U. Increasing frequencies and changing characteristics of heavy precipitation events threatening infrastructure in Europe under climate change. *Nat. Hazards Earth Syst. Sci.* **2017**, *17*, 1177–1190. [CrossRef]
18. Ibrahim, N.A.; Alwi, S.R.W.; Manan, Z.A.; Mustaffa, A.A.; Kidam, K. Risk matrix approach of extreme temperature and precipitation for renewable energy systems in Malaysia. *Energy* **2022**, *254*, 124471. [CrossRef]
19. Bezirgiannidis, A.; Chatzopoulos, P.; Tsakali, A.; Ntougias, S.; Melidis, P. Renewable energy recovery from sewage sludge derived from chemically enhanced precipitation. *Renew. Energy* **2020**, *162*, 1811–1818. [CrossRef]
20. Black, A.W.; Mote, T.L. Characteristics of winter-precipitation-related transportation fatalities in the United States. *Weather Clim. Soc.* **2015**, *7*, 133–145. [CrossRef]
21. Bucar, R.C.B.; Hayeri, Y.M. Quantitative assessment of the impacts of disruptive precipitation on surface transportation. *Reliab. Eng. Syst. Saf.* **2020**, *203*, 107105. [CrossRef]
22. Safdar, F.; Khokhar, M.F.; Mahmood, F.; Khan, M.Z.A.; Arshad, M. Observed and predicted precipitation variability across Pakistan with special focus on winter and pre-monsoon precipitation. *Environ. Sci. Pollut. Res.* **2023**, *30*, 4510–4530. [CrossRef] [PubMed]
23. Yavuz, H.; Erdoğan, S. Spatial Analysis of Monthly and Annual Precipitation Trends in Turkey. *Water Resour. Manag.* **2012**, *26*, 609–621. [CrossRef]
24. Gonzalez-Gonzalez, M.A.; Guertin, D.P. Seasonal bean yield forecast for non-irrigated croplands through climate and vegetation index data: Geospatial effects. *Int. J. Appl. Earth Obs. Geoinf.* **2021**, *105*, 102623. [CrossRef]
25. da Silva, M.V.; Pandorfi, H.; da Rosa Ferraz Jardim, A.M.; de Oliveira-Júnior, J.F.; da Divincula, J.S.; Giongo, P.R.; da Silva, T.G.F.; de Almeida, G.L.P.; de Albuquerque Moura, G.B.; Lopes, P.M.O. Spatial modeling of rainfall patterns and groundwater on the coast of northeastern Brazil. *Urban Clim.* **2021**, *38*, 100911. [CrossRef]
26. Sigrist, F.; Künsch, H.R.; Stahel, W.A. A dynamic nonstationary spatio-temporal model for short term prediction of precipitation. *Ann. Appl. Stat.* **2012**, *6*, 1452–1477. [CrossRef]
27. BMKG. Analisis Dinamika Atmosfer Dasarian III Mei 2022. 2022. Available online: https://www.bmkg.go.id/iklim/dinamika-atmosfir.bmkg (accessed on 1 May 2022).
28. Hermawan, E.; Lubis, S.W.; Harjana, T.; Purwaningsih, A.; Risyanto; Ridho, A.; Andarini, D.F.; Ratri, D.N.; Widyaningsih, R. Large-Scale Meteorological Drivers of the Extreme Precipitation Event and Devastating Floods of Early-February 2021 in Semarang, Central Java, Indonesia. *Atmosphere* **2022**, *13*, 1092. [CrossRef]
29. Anselin, L. *Spatial Econometrics: Methods and Models*; Springerl: Berlin/Heidelberg, Germany, 1988; Volume 85.
30. LeSage, J. Spatial Econometrics Toolbox. In *Introduction to Spatial Econometrics*; CRC Press: Boca Raton, FL, USA, 1999; p. 273. Available online: http://www.spatial-econometrics.com/ (accessed on 1 May 2022).
31. Pebesma, E.; Graler, B. *Introduction to Spatio-Temporal Variography*; ifgi: Munster, Germany, 2017.
32. Gio, P.U.; Effendie, A.R. *Belajar Bahasa Pemrograman R*; USU Press: Denver, CO, USA, 2018.
33. Lu, G.Y.; Wong, D.W. An adaptive inverse-distance weighting spatial interpolation technique. *Comput. Geosci.* **2008**, *34*, 1044–1055. [CrossRef]
34. Kopczewska, K. *Applied Spatial Statistics and Econometric*; Routledge: Abingdon-on-Thames, UK, 2021.
35. Abdullah, A.S.; Ruchjana, B.N.; Toharudin, T.; Rosadi, R. Model SAR, Ekspansi SAR dan Plot Moran untuk Pemetaan Hasil Akreditasi Sekolah di Provinsi Jawa Barat. In *Prosiding Seminar Nasional Matematika dan Pendidikan Matematika*; UMS: Kota Kinabalu, Malaysia, 2015; pp. 935–943.
36. Ord, K. Estimation methods for models of spatial interaction. *J. Am. Stat. Assoc.* **1975**, *70*, 120–126. [CrossRef]
37. Smirnov, O.; Anselin, L. Fast maximum likelihood estimation of very large spatial autoregressive models: A characteristic polynomial approach. *Comput. Stat. Data Anal.* **2001**, *35*, 301–319. [CrossRef]

38. Robinson, P.M.; Rossi, F. Refinements in maximum likelihood inference on spatial autocorrelation in panel data. *J. Econom.* **2015**, *189*, 447–456. [CrossRef]
39. Qiu, F.; Ding, H.; Hu, J. Asymptotic Properties of Quasi-Maximum Likelihood Estimators for Heterogeneous Spatial Autoregressive Models. *Symmetry* **2022**, *14*, 1894. [CrossRef]
40. Lawrence, K.D.; Klimberg, R.K.; Lawrence, S.M. *Fundamentals of Forecasting Using Excel*; Industrial Press Inc.: New York, NY, USA, 2009.
41. Zhang, C.; Hu, C.; Wu, T.; Zhu, L.; Liu, X. Achieving Efficient and Privacy-Preserving Neural Network Training and Prediction in Cloud Environments. *IEEE Trans. Dependable Secur. Comput.* **2022**, *20*, 4245–4257. [CrossRef]
42. Hu, C.; Zhang, C.; Lei, D.; Wu, T.; Liu, X.; Zhu, L. Achieving Privacy-Preserving and Verifiable Support Vector Machine Training in the Cloud. *IEEE Trans. Inf. Forensics Secur.* **2023**, *18*, 3476–3491. [CrossRef]